

Effect of Heat Treatment on Microstructure and Creep Behavior of Fe-40Ni-24Cr Alloy

Maureen Mudang, Esah Hamzah, Hamid Reza Bakhsheshi-Rad and Filippo Berto

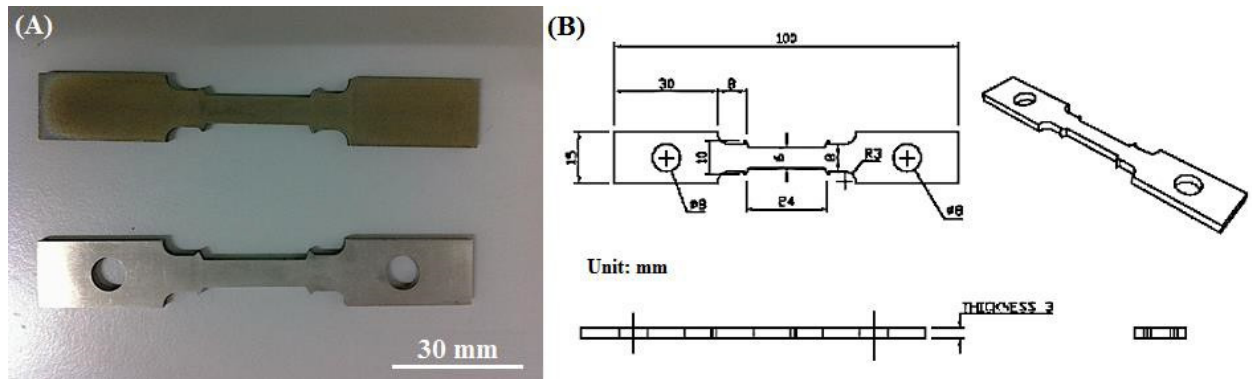


Figure S1. (A) Creep specimens and (B) Schematic diagram of creep specimen dimension.



Figure S2. (A) High temperature creep machine and (B) Creep test setup for Fe-Ni-Cr alloys.

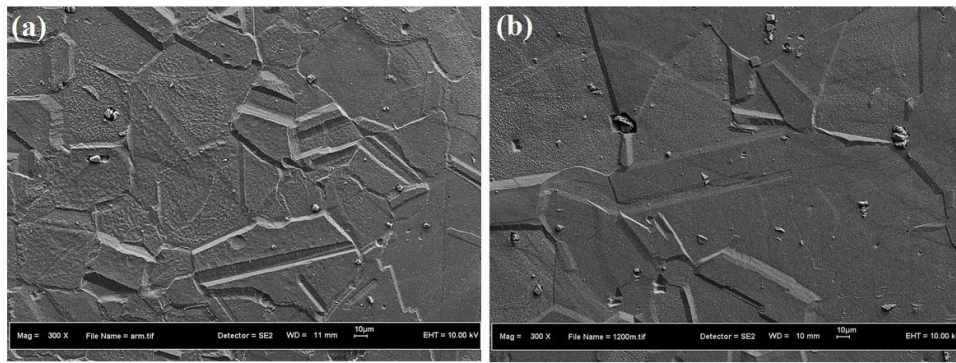


Figure S3. FESEM images of a) as-received Fe-40Ni-24Cr and b) solution treated Fe-40Ni-24Cr at 1200°C

Fig. S4 presented in supporting information shows the elemental mapping analysis conducted on the precipitates and matrix. The presence of titanium and niobium rich precipitates on the as-received and selected heat-treated Fe-40Ni-24Cr alloy were also supported by field FESEM supported with EDX element mapping analysis. High color concentration on titanium (Ti) and niobium (Nb) elements were detected at the titanium and niobium rich precipitates region, and they were distributed in the matrix and grain boundaries.

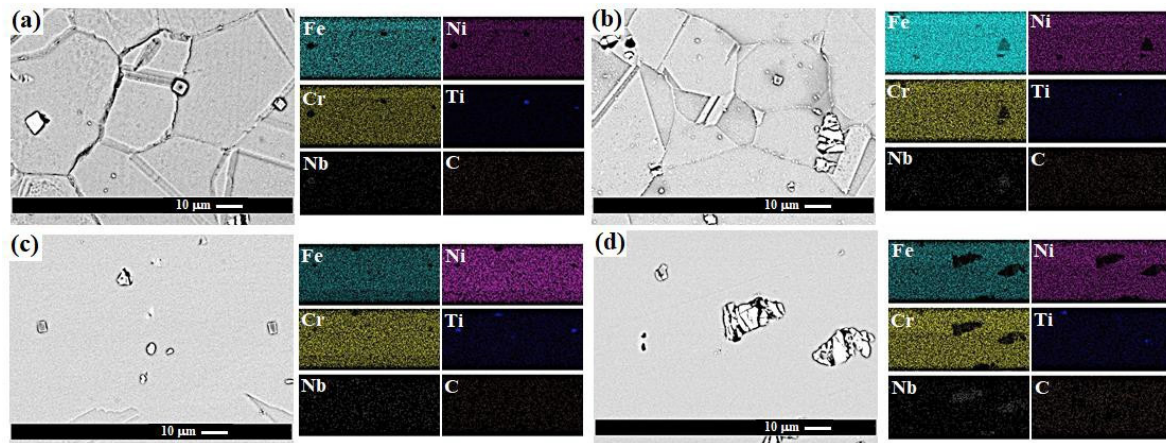


Figure S4. FESEM images with EDX elemental mapping analysis of Fe-40Ni-24Cr; (a) As-received, and heat-treated sample at different temperature (b) 950 °C, (c) 1050 °C and (d) 1250 °C.

Fig. S5 a-h presented in supporting information shows the XRD patterns of the as-received and heat-treated Fe-40Ni-24Cr alloy. Austenite peaks were present for the as-received and all of the heat-treated specimens. Besides austenite, several other weak peaks were identified as niobium carbide (NbC), niobium-titanium carbide ((Nb,Ti)C), titanium nitride (TiN), and titanium carbonitride (Ti(C,N)) precipitates [23, 46, 47]. Fig. S5 i and j depicted the heat treatment temperatures effect on the hardness value of Fe-40Ni-24Cr alloy. The hardness of heat-treated Fe-40Ni-24Cr alloy decreased with temperature and grain size. The hardness value of the as-received Fe-40Ni-24Cr was 182 HV. The as-received specimen heat-treated at 1177 °C possesses a grain size was 53 μm. At high-temperature treatment, the amount of dislocation was recovered. The hardness is resistant to deformation by indentation. Heat recovered specimens that were free

from dislocation and the grain boundaries are the reason which affected the hardness value [48]. Smaller grain size results in higher grain boundary areas, causing an increase in metal's capability to resist deformation. This is due to the grain boundaries reacting as a barrier for permanent deformation and resulting in a higher hardness value.

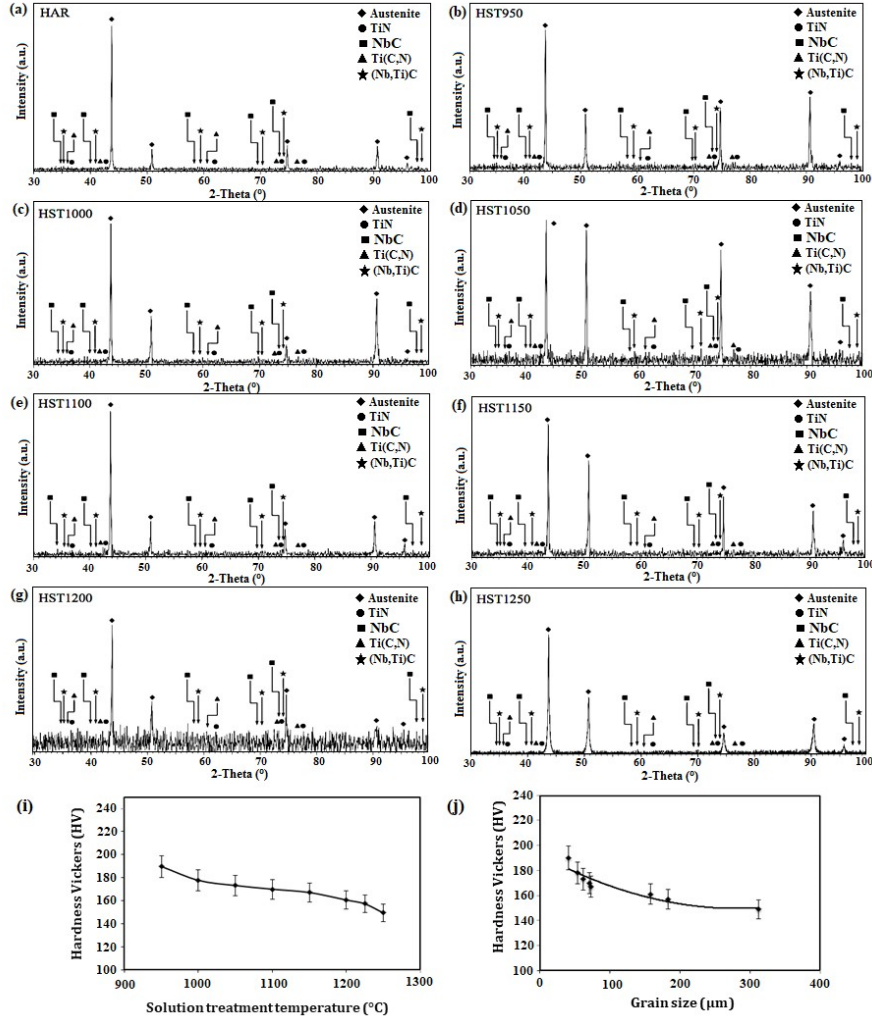


Figure S5. XRD pattern of Fe-40Ni-24Cr alloy, (a) As-received, and heat-treated sample at different temperature (b) 950 °C, (c) 1000 °C, (d) 1050 °C (e) 1100 °C, (f) 1150 °C, (g) 1200 °C and (h) 1250 °C and (i) hardness versus heat treatment temperature and (j) hardness versus grain size.

Fig. S6 shows the FESEM images of the recrystallized grains at the creep necking region. Clearly, recrystallized grains can be observed at high magnification. Results showed that intergranular rupture mode occurred where the crack propagated along the recrystallized grain boundaries. Recrystallization occurred at the necking area along the rupture boundaries. Recrystallized grains can be observed in all specimens. Smaller grain sizes have a greater ratio of grain boundary surface area per unit volume. These caused dislocations to easily pile-up at the grain boundaries [33]. Recrystallization processes usually occur at the area with high dislocation density, especially at the grain boundaries and grain boundaries around the triple point. At the secondary stage (steady-

state) of the high temperature of creep, the specimens underwent constant strain-rate under high-temperature conditions. This phenomenon represents a balance between work hardening caused by dislocation and dynamic recovery process caused by temperature. High-temperature creep is also considered a hot-working process (high temperature and high strain-rate). It requires an appreciation of both dynamic recovery and recrystallization processes, which only occur at high strain rate conditions. Dynamic recovery involves the rearrangement of dislocation to lower their stored energy. The dislocation rearrangement can occur by the annihilation of dislocation line length in the subgrain interior [34].

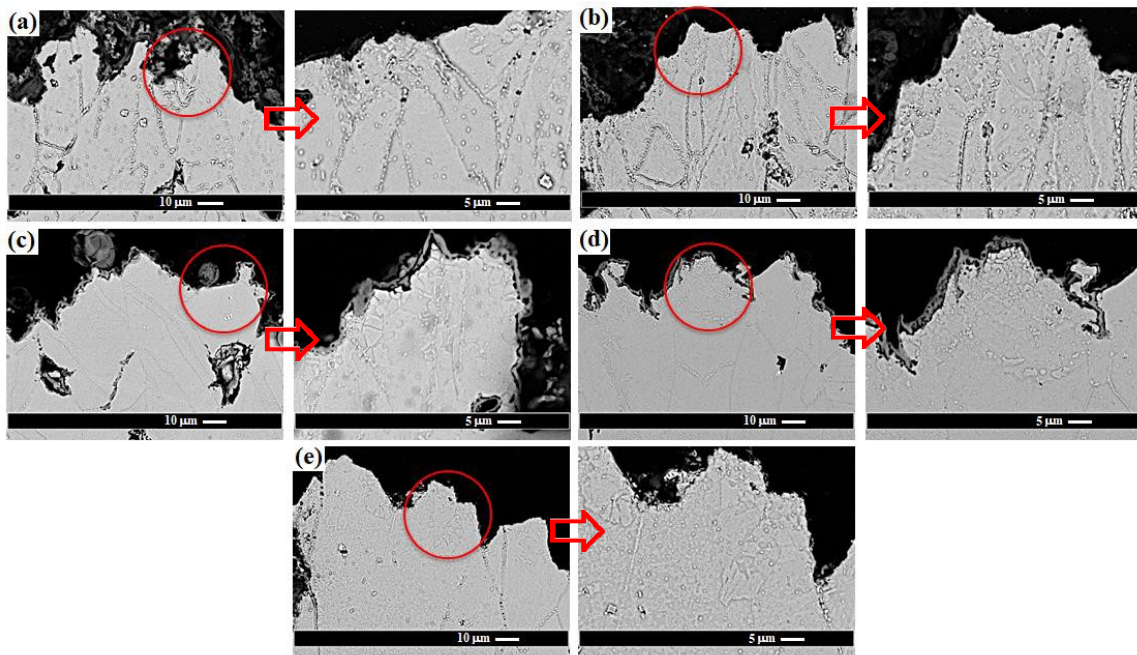


Figure S6. Cross-sectional FESEM micrographs of Fe-40Ni-24Cr after creep test at 800 °C under 100 MPa stresses (a) as-received, and heat-treated sample at different temperature (b) 1050 °C, (c) 1200 °C, (d) 1225 °C and (e) 1250 °C.

The presence of niobium and titanium-rich precipitates in the as-received and heat-treated creep specimens was verified by FESEM image and elemental mapping, as shown in Fig. S7 presented in supporting information. A high concentration of titanium (Ti) and niobium (Nb) elements were detected on the precipitates. A high concentration of chromium (Cr) element detected along the grain boundaries was identified as chromium-rich carbide (Cr_{23}C_6) precipitates. Voids formed at the Cr_{23}C_6 matrix interface located at the grain boundaries can clearly be observed in the figure. Voids are formed from the dislocations pile-up at the grain boundaries and contributed to excessive grain boundary crack. Triple junction boundary cracks and voids around titanium and niobium rich precipitates can also be observed.

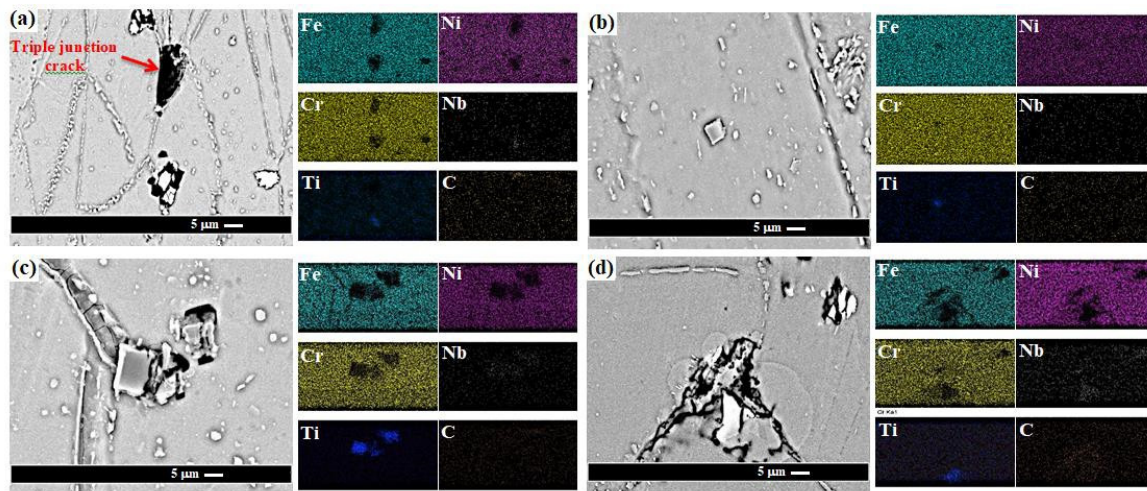


Figure S7. FESEM micrographs and corresponding EDX elemental mapping analysis of Fe-40Ni-24Cr after creep test at 800 °C under 100 MPa stresses (a) as-received, and heat-treated sample at different temperature (b) 1050 °C, (c) 1200 °C, and (d) 1250 °C.

Fig. S8 presented in supporting information shows the XRD patterns of the as-received and heat-treated Fe-40Ni-24Cr after undergoing a creep test at 800 °C and 100 MPa of stress. From the XRD patterns, the most intense five peaks were referred to as austenite. After undergoing hot deformation, several other small peaks were identified as Cr_{23}C_6 , TiN, Ti(C,N), NbC, and (Nb,Ti)C precipitates. The peaks for the precipitates were small due to the small number of precipitates present. The formation of stable types of M_{23}C_6 (chromium-rich) carbides is from the carbon in the material or decomposition of primary MC type carbides, where M is titanium, niobium, or tungsten and tantalum during high-temperature service. The aforesaid precipitates are present in the material before and after high-temperature creeps test.

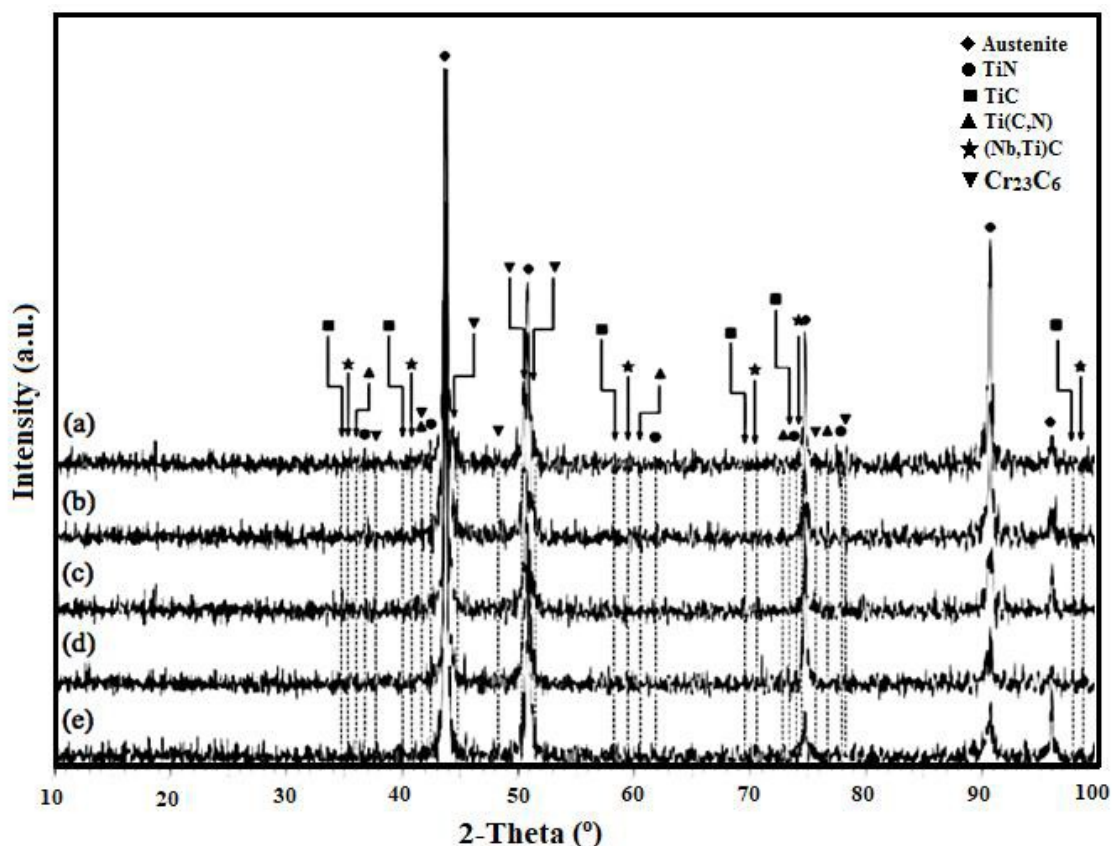


Figure S8. X-ray diffraction spectra of Fe-40Ni-24Cr after creep test at 800 °C under 100 MPa stresses of stress; (a) as-received, and heat-treated sample at different temperature (b) 1050 °C, (c) 1200 °C, (d) 1225 °C and (e) 1250 °C.

Fig. S9 presented in supporting information shows the FESEM micrographs supported with EDX elemental mapping analysis of Fe-40Ni-24Cr alloy after undergoing a creep test at 900 °C. A high concentration on Ti and Nb elements was detected at the blocky precipitates, as shown in Fig. S9. A slightly higher concentration of Cr element was detected along the grain boundaries, which determined as Cr_{23}C_6 precipitates. The concentration on Cr element along the grain boundaries is not very clear due to the Cr element is the tone of the major element based on the material. Voids and cracks (red arrows) around the blocky precipitates and Cr_{23}C_6 carbides can also be observed.

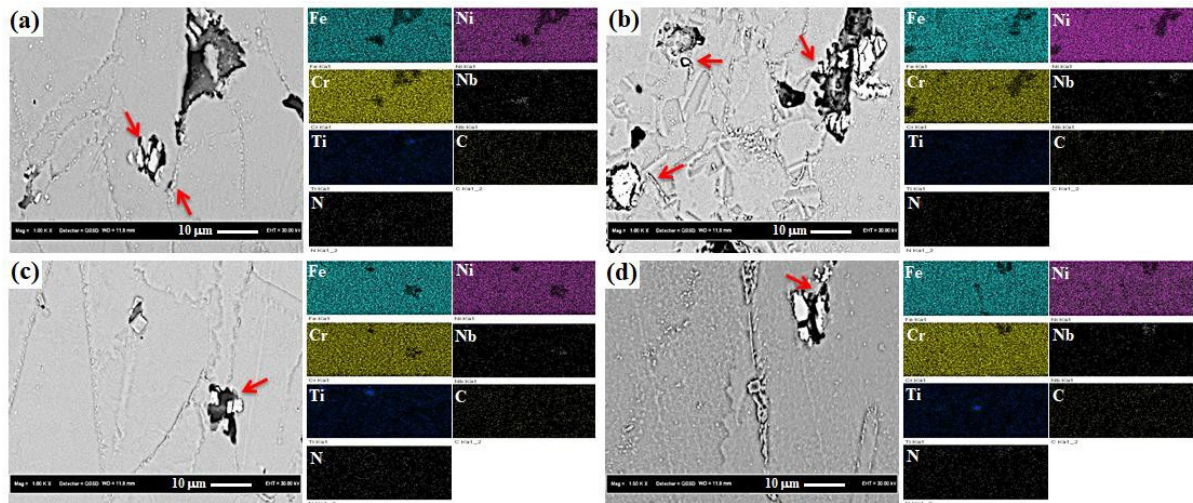


Figure S9. FESEM micrographs and corresponding EDX elemental mapping analysis of Fe-40Ni-24Cr after creep test at 900 °C under 100 MPa stresses (a) as-received, and heat-treated sample at different temperature (b) 1050 °C, (c) 1200 °C, and (d) 1250 °C.

Fig. S10 shows the rupture surface of alloy Fe-40Ni-24Cr after undergoing a creep test at 900°C. The figure shows the dimple rupture characteristic of micro-void coalescence and micro-crack. Due to the high test temperature, all rupture surface show dimple rupture. Dimple type of rupture surfaces indicated a ductile rupture manner, which is characterized by a large amount of deformation. The percentage of elongation for the as-received specimen was 44%. The percentage of elongation for heat-treated specimen was 53% for specimen heat-treated at 1050 °C, 46% for specimen heat-treated at 1200 °C, 43% for specimen heat-treated at 1225 °C, and 42% for specimen heat-treated at 1250 °C as shown in Fig. S10f. Total elongation significantly decreases with an increase in grain size. The results were in agreement with the critical length criterion for intergranular creep rupture [24] found to be applicable in Ni-Cr wrought alloy and 316 stainless steel. The grain size dependence of creep elongation is essentially due to the effect of grain size in the tertiary stage of the creep test. The tertiary creep stage involved the growth and inter-linkage of cracks and led to the final rupture.

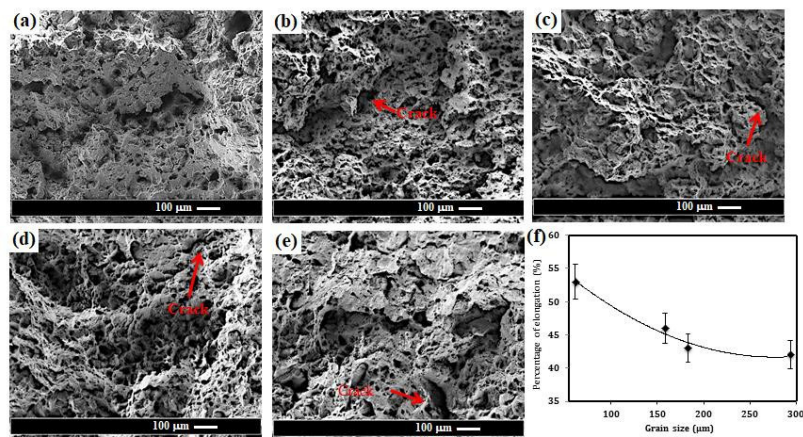


Figure S10. SEM micrographs of rupture surface of (a) as-received, and heat-treated sample at different temperature (b) 1050 °C, (c) 1200 °C, (d) 1225 °C and (e) 1250 °C and (f) percentage of elongation versus grain size of heat-treated Fe-40Ni-24Cr after creep test at 900°C and under 100 MPa stresses.

Fig. S11 presented in supporting information exhibits the X-ray diffraction patterns of the as-received and heat-treated Fe-40Ni-24Cr after undergoing a creep test at 900 °C and 100 MPa of stress. The most intense five peaks were identified as austenite. The austenite peaks were identified by referring to the PDF pattern number 00-031-0619. Cr₂₃C₆, TiN, Ti(C,N), NbC, and (Nb,Ti)C precipitates were found before and after the high-temperature creeps test. The peaks for these precipitates were very small due to the small amount of precipitates presence. It is worth noting that these carbides can hinder grain boundary sliding and migration during high temperature service.

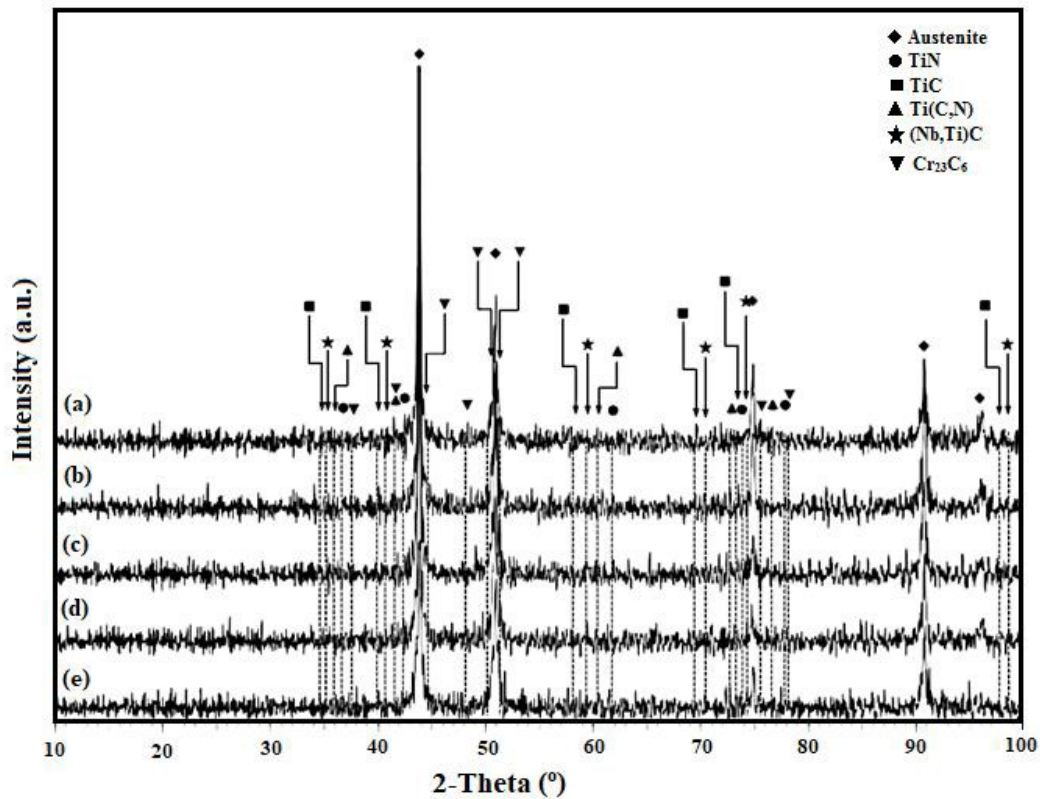


Figure S11. X-ray diffraction spectra of Fe-40Ni-24Cr after creep test at 900 °C under 100 MPa stresses of stress; (a) as-received, and heat-treated sample at different temperature (b) 1050 °C, (c) 1200 °C, (d) 1225 °C and (e) 1250 °C.

Table S1 Chemical composition of Fe-40Ni-24Cr (Haynes HR120)

Element	Fe-40Ni-24Cr (Haynes HR120) (wt.%)
Iron (Fe)	Balance
Nickel (Ni)	40.45
Chromium (Cr)	24.11
Carbon (C)	0.048
Silicon (Si)	0.441
Manganese (Mn)	0.702
Titanium (Ti)	0.029
Copper (Cu)	0.114
Sulfur (S)	<0.001
Aluminum (Al)	0.08
Niobium (Nb)	0.441
Molybdenum (Mo)	0.249
Cobalt (Co)	0.169
Boron (B)	0.0014
Phosphorus (P)	0.014
Vanadium (V)	0.041
Tungsten (W)	0.053
Nitrogen (N)	0.206